Proceedings of the ASME 2022
International Mechanical Engineering Congress and Exposition
IMECE2022
October 30-November 3, 2022, Columbus, Ohio

IMECE2022-97021

NUMERICAL SIMULATION FOR ANALYZING INTERFACIAL VELOCITY AND INTERFACIAL FORCES OF A BUBBLE MOTION IN TAPER MICRO GAP

Divyprakash Pal
Rochester Institute of Technology
Rochester, NY

Maharshi Shukla
Rochester Institute of Technology
Rochester, NY

Isaac Perez-Raya
Rochester Institute of Technology
Rochester, NY

Satish Kandlikar
Rochester Institute of Technology
Rochester, NY

ABSTRACT

Heat transfer due to the convective boiling mechanism in the microchannel plays an important role in heat transfer during boiling. Therefore, it is relevant to find ways to manipulate the vapor bubbles such that convection heat transfer is enhanced. This numerical study investigates the effects of different geometrical parameters on bubble movement through a micro tapered gap. The objective is to identify an optimal configuration such that the bubble moves at the fastest possible speed when it travels through the micro gap. To conduct this research a model is created using ANSYS-Fluent which uses the Volume of Fluid (VOF) interface tracking method. The multiphase VOF model tracks the air-water interface. A bubble is generated inside the microchannel in which fluid is flowing. The overall domain of the model consists of the surface at the bottom, having an orifice through which the air bubble is generated. Three different cases of an angled tapered surface are created 5°, 10°, and 15°. The airflow rate is kept constant throughout each simulation. Simulation results show the impact of the tapered angle on the bubble's flow movement and flow direction. Liquid and air velocity contours can be used to analyze the flow. The impact of the taper angles on the movement and flow direction of the air bubble is discussed. It is observed that the performed simulations help to better understand the experimental observation of bubble motion; the simulations give clear evidence of the fluid dynamic behavior along the tapered microchannel.

Keywords: Volume of fluid, microchannel, taper micro gap

NOMENCLATURE

$\vec{g}$	$gravity\ m/s^2$
ρ	density (kg/m^3)
t	time (s)
$\vec{u}$	velocity vector (m/s)
μ	liquid viscosity (Pa s)
F_q	fluid volume fraction (dimensionless)
κ	curvature of the interface

Subscripts

g	gas phase
l	liquid phase

1. INTRODUCTION

Boiling is one of the most efficient modes of heat transfer and it is used in applications such as power generation, propulsion, electronics cooling, chemical processes, etc. Improving heat-transfer performance helps with energy system efficiency and stability. Understanding bubble behavior at different surface configurations is important to enhance heat dissipation. The present work employs computer simulation to understand bubble growth on a tapered surface.

Since the pioneering work of Shiro [1] was published, pool boiling has so far garnered massive interest as a passive technique of heat transfer. Bubble growth, departure, and interaction with the preceding bubble were experimentally studied using high-speed cameras by Siedel [2]. The work brings to light that the departing bubble has a significant impact on the following bubble. The growth of the vapor bubble in terms of

volume is directly influenced by the increase in advancing contact angle. This was numerically studied by Abhijit Mukherjee and Kandlikar [3] and concluded that an increase in the advancing contact angle increases the rate of vapor volume growth. A similar agreement was achieved by Son et al. [4] where a departing bubble was seen to increase in size with an increase in contact angle and wall superheat.

Significant work has been done so far to enhance the heat transfer in pool boiling with varying parameters like heated surface, using different geometries, fluid selection, etc. Surface enhancement using nanostructured horizontal interfaces was experimentally tested by S. Launay [5]. Performances of smooth, rough silicon, silicon-etched, and carbon Nano-tubes (CNT) based pin-fin arrays were analyzed and reported. As compared to the smooth surfaces the CNT-enabled nanostructures improved heat transfer but at a very low superheat, thus showcasing the influence of surface and fluid interaction. Another study on the influence of surface roughness and shape of fins on pool boiling by Hubner and Kunstler [6] demonstrated that the trapezoidal-shaped geometry of fins had better heat transfer over plain tubes. An experimental study was carried out by Das et al. [7] to investigate the heat transfer enhancement by using artificial distinct nucleation sites. From the boiling curve of the micro-drilled surface having 5mm, 7.5mm, and 10mm pitch it could be seen that there was an increase in heat flux as compared to the plain surface. In the nucleate pool boiling the isolated bubbles keep on replacing the heated liquid at the bottom heated surfaces with a new influx of cold fluid. This makes the bubble act as a pump, and with the increase of the nucleation site density, the base area per site decreases. Thus, although the heat transfer increases with nucleate site density, continuous increment in nucleate site density eventually leads to decreased rate of heat transfer.

There has been extensive research carried out in terms of geometrical variation in flow boiling as well as in pool boiling especially in microchannels. Kandlikar [8] studied the flow instabilities due to nucleation in microchannels using high-speed visual observations. Mukherjee and Kandlikar [9] numerically studied bubble growth in a microchannel and proposed tapered microchannels to reduce instabilities. The geometry was further evaluated based on its effect on pressure recovery by Kalani and Kandlikar [10] and showed an effective decrease in pressure drop in flow boiling. This particular geometry was modified into a converging and diverging manifold by Moreira et al. [11]. They stated that due to an increase in the flow constraint, the pressure drop of converging and diverging gaps was higher than that of uniform gaps, but a significant improvement in heat transfer was also obtained with both tapered gaps, and the converging configuration presented the best results. These findings were tested for pool boiling by Chauhan and Kandlikar [12] and they hypothesized that a self-sustained flow using tapered micro gaps eliminates the need for an external pump and transforms a pool boiling system into a pump less flow boiling system with significantly higher heat transfer potential. A further continuation of this study by Chauhan and Kandlikar [13] showed that dual tapered geometry in pool boiling could achieve high heat dissipation efficiency using dielectric fluid HFE7000. Numerous works have been done to study pool boiling numerically [14] [15] [16] [17] which showed that numerical studies have shown conformity with experimental work. Using a similar approach this paper presents a Computational Fluid Dynamics (CFD) based model using the source ANSYS FLUENT 2021 R1 to study the various parameters of bubble generation, growth, and departure in a tapered model. The geometries created are inspired by works reported in [9] [10] [11] [12].

The present work performs a numerical simulation of bubble growth along a tapered surface. The main objective of the present work is to study the impact of the tapered angle on the flow behavior and flow direction of the bubble. The tapered surface considers three inclination angles and a constant flow rate. An experimental test with air injection was performed to validate the simulation results and good agreement was found. The 5^o tapered angle had the shortest time for a bubble departure for the same flow rate according to simulation data.

2. MATERIALS AND METHODS

The 2D numerical simulation using taper geometry was performed on an ANSYS Fluent 2021 R1 commercial CFD package. The tapered surface considers three inclination angles of 5^o, 10^o, and 15^o at a 3 ml/min flow rate. Also, the simulation were run and bubble shapes were analyzed until a steady bubble growth process and cycle was observed (usually after the fourth departed bubble a steady cycle was achieved). The following sections describe the computational domain, the boundary conditions, the simulation parameters, and the experimental setup used for validation.

2.1 Computational domain and grid

The number of computational cells was 176243, 182730, 187118 for the 5^o, 10^o, and 15^o degree tapered angled microchannels. The mesh has a minimum cell size of 4e-05 and a maximum cell size of 5e-04.

2.2 Boundary conditions

The enclosure that is the computational domain consists of water-liquid along with air injection at an orifice. Figure 1 shows the boundary conditions that were used to set up the simulation model in ANSYS-Fluent. At the top of the enclosure is a pressure outlet. The orifice at the bottom of the enclosure is the velocity inlet. Boundaries that are the left side, right side, and bottom are all defined as walls. Table 1 shows relevant parameters used to define the simulation domain. It is important to observe that the simulation uses three different taper angles and in all three cases the simulation uses constant flow rates of 3 ml/min.

2.3 Simulation settings

The ANSYS Fluent solves the governing equations for continuity, momentum, and volume of fluid. The simulation software solves the volume-of-fluid (VOF) interface tracking equation and uses the sharp interface VOF model. The SIMPLE

algorithm was employed to handle the pressure velocity coupling. The gradient of all flow variables was calculated using the green-gauss cell-based method, while the momentum terms in the governing equation were approximated by the QUICK scheme. Transient simulations were utilized in time by a global courant number ranging less than 0.1, which ensured the stability of the numerical approach and the converging criteria of the model.

2.4 Governing Equations

The conservation of mass equation is:

$$\nabla \cdot \vec{u} = 0 \tag{1}$$

where ∇ is the gradient operator.

The conservation of momentum equation is:

$$\frac{\partial(\rho\overrightarrow{v})}{\partial t} + \nabla \cdot (\rho\vec{v}\vec{v}) = -\nabla p + \nabla \cdot \{\mu[\nabla\vec{v} + (\nabla\vec{v})^T]\} + F_s + \rho\vec{g} \tag{2}$$

where F_s corresponds to the surface tension applied to the cells that have an interface.

The VOF interface tracking equation is:

$$\frac{\partial F_q}{\partial t} + \vec{u}_q \cdot \nabla F_q = 0 \tag{3}$$

where F_q is the volume-fraction of air in the computational cells.

$$\sum_{q=1}^{2} F_q = 1 \tag{4}$$

This constraint will be used to solve for the primary phase since equation (3) does not account for the volume of fractions in the primary phase.

The density and viscosity of the gas and liquid phases are estimated with the volume fractions. The following expressions show the adopted formulation:

$$\rho(\vec{x},t) = F(\vec{x},t)\rho_l + [1 - F(\vec{x},t)]\rho_g \tag{5}$$

$$\mu(\vec{x},t) = F(\vec{x},t)\mu_l + [1 - F(\vec{x},t)]\mu_g \tag{6}$$

where ρ is density and μ is viscosity.

Surface tension force is included in the momentum equation using the VOF values. This force acts to balance the forces at the interface of the two fluids. Equation 7 gives the surface tension force.

$$F_s = \sigma \frac{\rho K \nabla F_1}{0.5\,(\rho_g + \rho_l)} \tag{7}$$

where,

$$k = \nabla \cdot \hat{n} \tag{8}$$

$$n = \nabla F_q \tag{9}$$

The surface tension effect is included which acts along with the interface between the phases. The surface tension is a constant.

2.5 Experimental setup

The experimental setup consists of a Masterflex L/S peristaltic pump that can pump a set flow rate of air through a thin tube into a pool of water. The air inlet has a diameter of 1 mm and the center of this air inlet is located 1 mm from the tapered inlet. The taper inlet gap is 1 mm and the angle is 5°. The airflow rate was set at 3 ml/min for the experiments and a Photron high-speed camera was used to record the squeezing air bubble and the bubble movement was captured at 2000 fps.

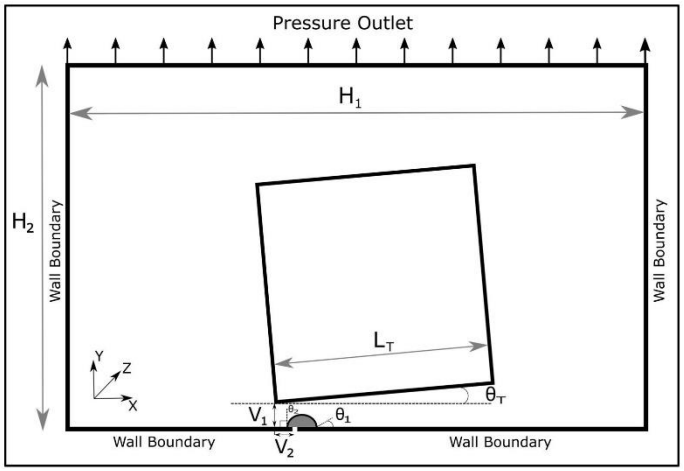

FIGURE 1: SKETCH OF THE COMPUTATIONAL DOMAIN.

Parameter	Symbol	Value
Orifice size	D	1 [mm]
Domain length	H_1	31.9 [mm]
Orifice distance	V_2	1 [mm]
Taper gap	V_1	1 [mm]
Domain height	H_2	20 [mm]
Taper length	L_T	12 [mm]
Taper angle	θ_T	5°,10°,15°
Leading angle	θ_1	60°
Trailing angle	θ_2	90°

TABLE 1: RELEVANT PARAMETERS IN THE SIMULATION.

3. RESULTS

The results section covers the effect of taper angles on the movement and flows direction of the air bubble. The simulations produced a visualization of bubble dynamics. The flow was studied using volume fraction and velocity contours.

3.1 Mesh analysis

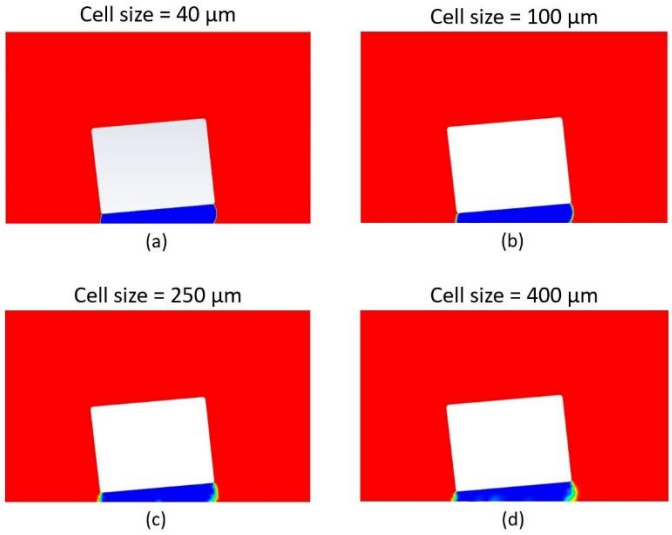

FIGURE 2: 5º TAPER ANGLE AT t = 0.75 s.

Mesh Cell Size (μm)	Number of Cells
40	176243
100	30377
250	6299
400	3253

TABLE 2: MESH CELL SIZE AND NUMBER OF CELLS.

The mesh sensitivity test was performed for the case of 5º tapered angle. Figure 2 shows the interface of the bubble generated at t = 0.75 s for four different mesh sizes. The cell sizes and the number of cells have been documented in Table 2. The results showed that the interface shares an inverse relation with the cell size. With the increase in mesh cell size, the interface tends to degrade further. The cell size of 40 μm was used for all the studies reported in the present work. In addition, the Courant number remained below 0.25 in all the simulations to ensure a correct time step size.

3.2 Validation of the numerical simulation

Figures 3 and 4 compare the different stages of the bubble expansion given by the simulation and experiments. The flow rate is 3 ml/min and the angle is 5º. The gray color contours on the top show experiments whereas the bottom side show the volume fractions (blue color represents air, red color represents water, and the interface shows a transition color from blue to red), each figure shows the time on the top. Figure 3 shows the initial stage of bubble growth from 0.03 s to 0.98 s for simulation whereas Figure 4 shows the final stage from 1.05 s to 1.14 s. Results indicate a good agreement between the experiment and simulations in terms of bubble shape and behavior. The bubble departs in 0.95 s according to the experimental data, while the bubble departs in 1.14 s according to the numerical calculations. The discrepancy between the departure times is 20% which is acceptable. The difference might be due to the 3D experiment effects that were ignored by the simulation. In addition, further testing needs to be done with higher flow rates where the 3D effects of bubble expansion along the z-axis may be more prominent.

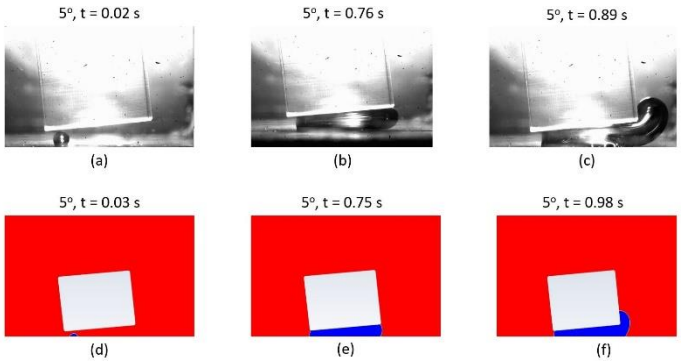

FIGURE 3: 5º TAPER ANGLE INITIAL STAGE. (a), (b), (c) REPRESENT THE EXPERIMENTAL RESULTS AND (d), (e), (f) REPRESENT THE SIMULATION RESULTS.

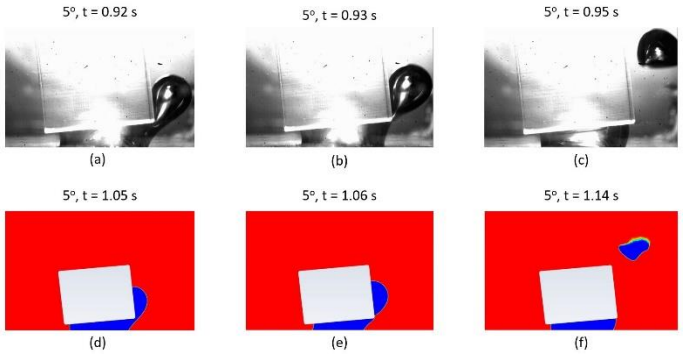

FIGURE 4: 5º TAPER ANGLE FINAL STAGE. (a), (b), (c) REPRESENT THE EXPERIMENTAL RESULTS AND (d), (e), (f) REPRESENT THE SIMULATION RESULTS.

The numerical results in Figures 3 and 4 show the evolution of a bubble in a tapered microchannel at an inclination angle of 5º. The figures show six different time frames selected to illustrate the bubble shape from the conception to its departure. At the time of 0.03 s, the bubble is still growing and is not yet in contact with the tapered surface. At a time equal to 0.75 s, the bubble continues to grow due to continuous injection of air and creates a slug once it is in contact with the taper and keeps moving forward in the right direction towards the diverging end. At t = 0.98 s the bubble has completely covered the taper area and is still moving at the right end of the taper. At time t = 1.05 s the bubble has formed a neck at the edge of the taper and looks

set to depart. The departure of the bubble can be seen at t = 1.06 s and the bubble fully leaves the tapered surface at 1.14 s.

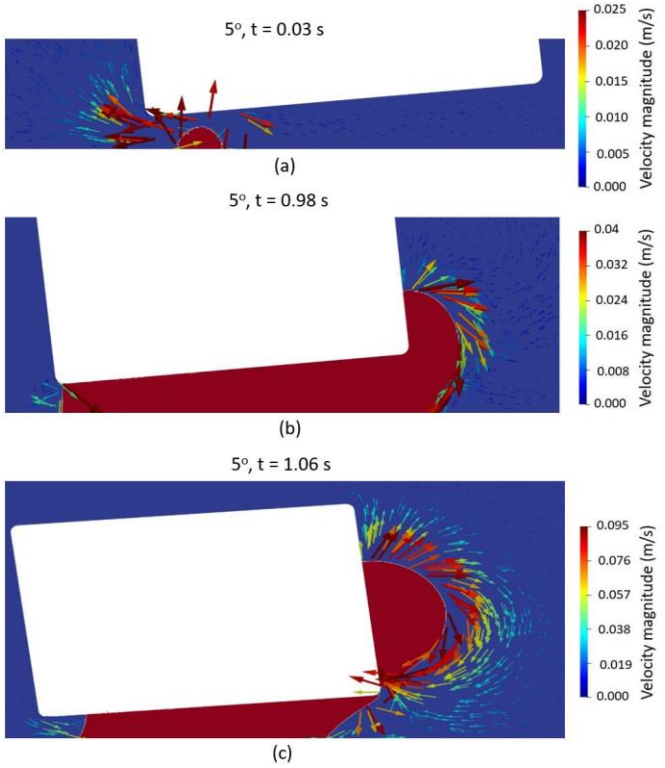

FIGURE 5: 5° TAPER ANGLE VELOCITY VECTOR FROM t = 0.03 s to t = 1.06 s.

Figure 5 shows the velocity vector of the 5° case. Initially, the formation of the bubble shows the velocity vectors of maximum magnitude pushing the liquid towards the convergent side. As the bubble grows the surface tension and the leading edge angle helps move the bubble towards the divergent end. At t = 0.98 s, the velocity vectors seem to be creating a circular motion forcing the liquid to move in the lower section of the leading edge of the bubble. This results in the bubble moving towards the upper section of the divergent end. This change in direction eventually leads to the change in magnitude at the convergent end where the value seems to be lower as compared to the formation of a bubble. The bubble can be seen separating at t = 1.06 s, where the velocity vectors at the leading edge are pushing the liquid away, while the trailing edge sees the velocity vectors of higher magnitude helping in the separation of the bubble from the preceding bubble. Similar patterns were observed for the cases with 10° and 15° tapered angles.

Figure 6 shows the growth and departure of a bubble at an inclination angle of 10°. The figure shows six different time frames selected to illustrate the time from the conception of the bubble to its departure. At t = 0.06 s the bubble shows a similar pattern of growth relative to the 5° degree tapered angle case. Also at the time of 0.608 s, it can be seen that the bubble continues to grow and it goes through a squeezing effect between the taper and the bottom surface. The bubble then moves towards the diverging edge of the tapered microchannel. The bubble forms a similar neck pattern as that of the 5° case. The departure of the bubble can be seen at t = 1.38 s and it fully leaves the tapered surface at 1.44 s. The results of the simulation show a larger time of departure in the 10° relative to the 5° case, which might be due to the increase in flow area with a higher angle.

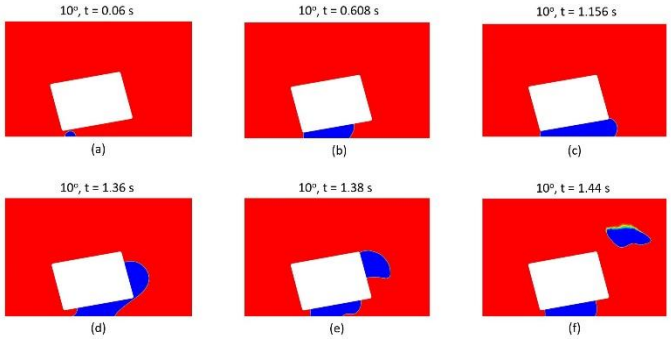

FIGURE 6: 10° TAPER ANGLE INITIAL AND FINAL STAGE FROM t = 0.06 s TO t = 1.44 s.

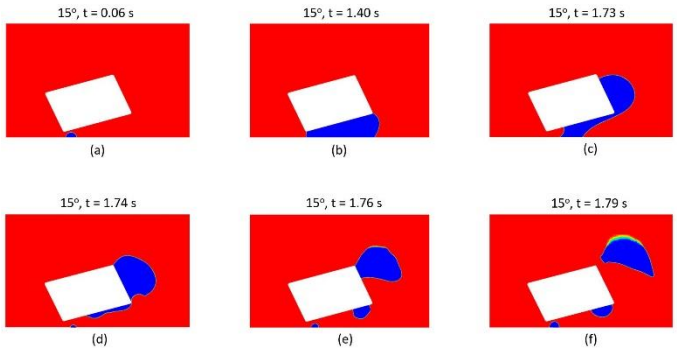

FIGURE 7: 15° TAPER ANGLE INITIAL AND FINAL STAGE FROM t = 0.06 s TO t = 1.79 s.

Figure 7 shows the growth and departure of a bubble at an inclination angle of 15°. The images show the bubble from conception to the point where the bubble departs. At t = 0.06 s the bubble is not in contact with the tapered surface. Similar to previous cases when the bubble comes in contact with the tapered surface at t = 1.40 s, the bubble moves towards the divergent end. The time for the bubble to reach the divergent edge of the taper is relatively higher compared to the previous cases.

This can be attributed to the more area available for the bubble to expand at the same flow rate. The volume of the bubble as it moves to the right becomes larger creating a longer interface between the liquid and air. Eventually, the bubble grows large enough and can neck and depart the microchannel which can be seen from t = 1.74 s to t = 1.79 s. In contrast to prior occurrences, the subsequent bubbles that are generated after the initial bubble separates are different individual bubbles that do not come in touch with the newly formed bubble. The results of the simulation illustrate that with a high tapered angle of 15° the bubble still moves towards the divergent end of the tapered channel.

4. CONCLUSION

The present work performed a simulation of bubble growth in a taper microchannel. The simulation was validated against the experiments and good agreement was observed in terms of bubble growth and bubble shapes. Also, a 20% error in the bubble departure time was observed, which is acceptable since the simulation neglects 3D effects. In addition, the simulation revealed bubbles traveling towards the diverging side with low or high taper angles.

The simulation results gave evidence of the fluid behavior during the bubble growth and departure process. It can be seen from the velocity vectors that fluid is pushed away towards the divergent edge as the bubble grows and gets ready to separate and depart. The surface tension creates fluid circulation and the leading and trailing edge angles help support the bubble movement towards the right side of the tapered surface. The bubble appears to be more inclined to migrate to the nearest zone of departure on the left at first, but after it makes contact with the tapered surface, it begins to expand on the right side. The fluid circulation also aids in the separation of the bubble from the preceding bubble and the bubble's departure.

Each of 5^o, 10^o, and 15^o have similar flow patterns and shows good accordance with each other by moving on the diverging side of the tapered microchannel. For the 5^o case, the bubble departs at t = 1.150 s, but when compared to the 10^o and 15^o the bubble reaches just the edge of the tapered geometry at t = 1.156 s and t = 1.40 s respectively. This confirms that the simulation work is accurate in simulating the real-world process of bubble departure being delayed due to additional bubble growth area. This also aids in comprehending the flow control that may be achieved by varying the tapered angle. Lower degrees of inclination can be employed to enhance the number of bubble departures for the same flow rate.

Results indicated that initially, the injected air tries to move the small bubble towards the converging zone. However, as the bubble continues to grow and interact with the tapered surface, results revealed the velocity magnitude on the trailing-edge decreases and the velocity magnitude on the leading-edge increases which makes the bubble move towards the diverging zone.

The 2D simulation is capable of producing experimental results. However, we are expanding the model to perform 3D simulations which will result in a better approximation of the actual bubble growth behavior in a tapered microchannel. A 2D model is easier to create and can be iterated multiple times within less span of time. The results help provide us a base to carry this work forward into the 3D analysis.

Overall the simulation closely reproduces experimental observations at the analyzed flow rate and gives evidence of the relevant parameters influencing the bubble behavior in the tapered micro-channel.

ACKNOWLEDGEMENTS

The authors gratefully acknowledge the support from the national science foundation under a CBET grant.

REFERENCES

[1] N. Shiro, *"The maximum and minimum values of the heat q transmitted from metal to boiling water under atmospheric pressure," Int. J. Heat Mass Transf., vol. 27, no. 7, pp. 959–970*, Jul. 1984, DOI: 10.1016/0017-9310(84)90112-1.

[2] S. Siedel, S. Cioulachtjian, and J. Bonjour, *"Experimental analysis of bubble growth, departure and interactions during pool boiling on artificial nucleation sites," Exp. Therm. Fluid Sci., vol. 32, no. 8, pp. 1504–1511*, Sep. 2008, DOI: 10.1016/j.expthermflusci.2008.04.004.

[3] A. Mukherjee and S. G. Kandlikar, *"Numerical study of single bubbles with dynamic contact angle during nucleate pool boiling," Int. J. Heat Mass Transf., vol. 50, no. 1, pp. 127–138,* Jan. 2007, doi: 10.1016/j.ijheatmasstransfer.2006.06.037.

[4] G. Son, V. K. Dhir, and N. Ramanujapu, *"Dynamics and Heat Transfer Associated With a Single Bubble During Nucleate Boiling on a Horizontal Surface," J. Heat Transf., vol. 121, no. 3, pp. 623–631*, Aug. 1999, DOI: 10.1115/1.2826025.

[5] S. Launay, A. G. Fedorov, Y. Joshi, A. Cao, and P. M. Ajayan, "*Hybrid micro-nano structured thermal interfaces for pool boiling heat transfer enhancement," Microelectron. J., vol. 37, no. 11, pp. 1158–1164*, Nov. 2006, DOI: 10.1016/j.mejo.2005.07.016.

[6] P. Hübner and W. Künstler, "*Pool boiling heat transfer at finned tubes: influence of surface roughness and shape of the fins," Int. J. Refrig., vol. 20, no. 8, pp. 575–582*, Dec. 1997, DOI: 10.1016/S0140-7007(97)00033-9.

[7] A. K. Das, P. K. Das, and P. Saha, *"Nucleate boiling of water from plain and structured surfaces," Exp. Therm. Fluid Sci., vol. 31, no. 8, pp. 967–977*, Aug. 2007, DOI: 10.1016/j.expthermflusci.2006.10.006.

[8] S. G. Kandlikar, "*Fundamental issues related to flow boiling in minichannels and microchannels," Exp. Therm. Fluid Sci., vol. 26, no. 2, pp. 389–407*, Jun. 2002, DOI: 10.1016/S0894-1777(02)00150-4.

[9] A. Mukherjee and S. G. Kandlikar, "*The effect of inlet constriction on bubble growth during flow boiling in microchannels," Int. J. Heat Mass Transf., vol. 52, no. 21, pp. 5204–5212*, Oct. 2009, doi: 10.1016/j.ijheatmasstransfer.2009.04.025.

[10] A. Kalani and S. G. Kandlikar, "*Effect of taper on pressure recovery during flow boiling in open microchannels with manifold using homogeneous flow model," Int. J. Heat Mass Transf., vol. 83, pp. 109–117,* Apr. 2015, doi: 10.1016/j.ijheatmasstransfer.2014.11.080.

[11] D. C. Moreira, G. Ribatski, and S. G. Kandlikar, "*Effects of Taper Configurations on Heat Transfer and Pressure Drop in Single-Phase Flows in Micro gaps," p. 6*, 2020.

[12] A. Chauhan and S. G. Kandlikar, *"Transforming pool boiling into self-sustained flow boiling*

through bubble squeezing mechanism in tapered micro gaps," Appl. Phys. Lett., vol. 116, no. 8, p. 081601, Feb. 2020, DOI: 10.1063/1.5141357.

[13] A. Chauhan and S. G. Kandlikar, *"Geometrical effects on heat transfer mechanisms during pool boiling in Dual Tapered Microgap with HFE7000," Int. J. Heat Mass Transf., vol. 183, p. 122165*, Feb. 2022, doi: 10.1016/j.ijheatmasstransfer.2021.122165.

[14] N. Minocha, J. B. Joshi, A. K. Nayak, and P. K. Vijayan, *"3D CFD simulation of passive decay heat removal system under boiling conditions: Role of bubble sliding motion on inclined heated tubes," Chem. Eng. Sci., vol. 145, pp. 245–265*, May 2016, DOI: 10.1016/j.ces.2016.02.015.

[15] Y. Liu, T. Olewski, and L. N. Véchot, *"Modeling of a cryogenic liquid pool boiling by CFD simulation," J. Loss Prev. Process Ind., vol. 35, pp. 125–134*, May 2015, DOI: 10.1016/j.jlp.2015.04.006.

[16] S. M. A. N. R. Abadi and J. P. Meyer, *"Numerical investigation into the inclination effect on conjugate pool boiling and the condensation of steam in a passive heat removal system," Int. J. Heat Mass Transf., vol. 122, pp. 1366–1382*, Jul. 2018, doi: 10.1016/j.ijheatmasstransfer.2017.12.093.

[17] C. P. Karthikeyan, G. Kalpana, V. Krishnamoorthy, and A. A. Samuel, *"Transient numerical analysis of thermophoresis and particle dynamics in a nanofluid – pool boiling conditions," J. Mol. Liq., vol. 301, p. 112459,* Mar. 2020, DOI: 10.1016/j.molliq.2020.112459.